# STELLAR ACTIVITY CYCLES

MAREK STĘŚLICKI

# GLOBALLY THE SUN IS A REMARKABLY CONSTANT STAR

- RMS variations in irradiance (observed bolometric flux), as measured from Earth orbit since 1978, are ≈ 0.04%
- The 0.04% RMS variations occur on time scales of decades and less,
  - the thermal relaxation timescale for the Sun's convection zone is $10^5$ years,
  - global magnetic fields "diffusion time" is $10^9$ years
- Solar magnetic field, evolving globally on decadal time scales!

# DIRECT OBSERVATIONS

- Direct observations of the magnetic field (Zeeman splitting, polarization) are possible only for few special targets (rapidly rotating and active), e.g. Ap stars

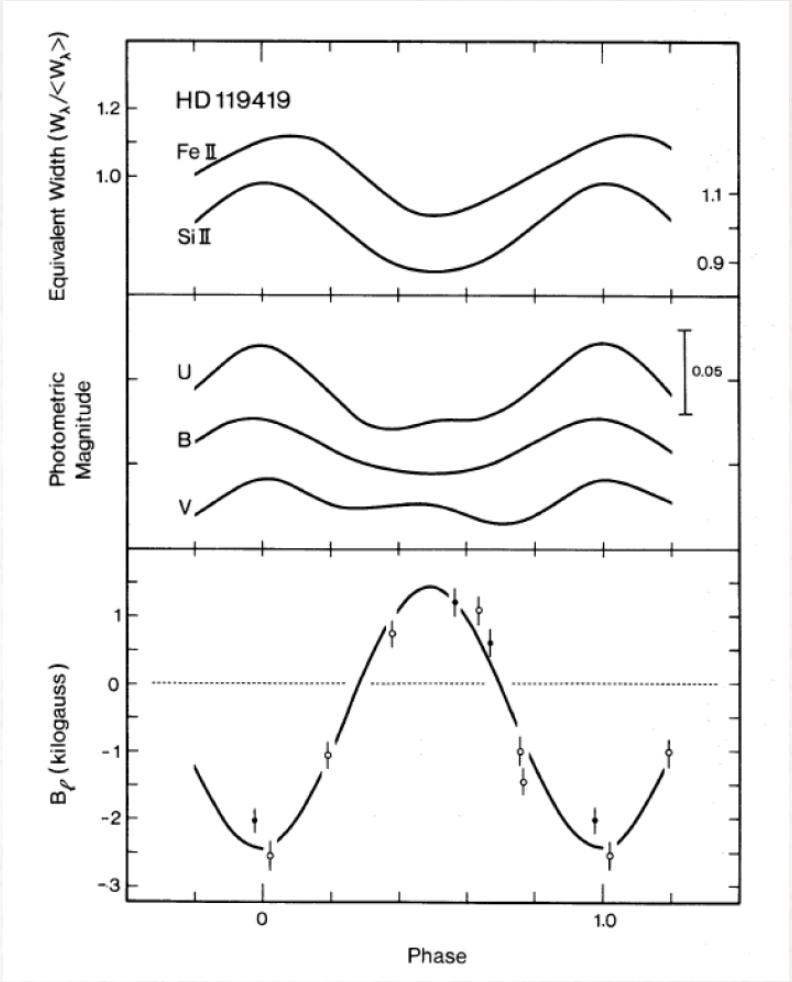


**Fig. 6.** Variations observed in the magnetic Ap star HD 119419 as a function of phase through the 2.60 d period. The curves show (from the top) the variations of equivalent width of Fe and Si lines, of brightness in the Johnson UBV bands, and of $\langle B_z \rangle$.

Landstreed (2008)

# PROXIES FOR MAGNETIC ACTIVITY ON SOLAR-LIKE STARS

Proxies:

Variable radiation in:

- chromosphere (optical, UV lines)
- transition region (UV)
- corona (EUV, X-ray)

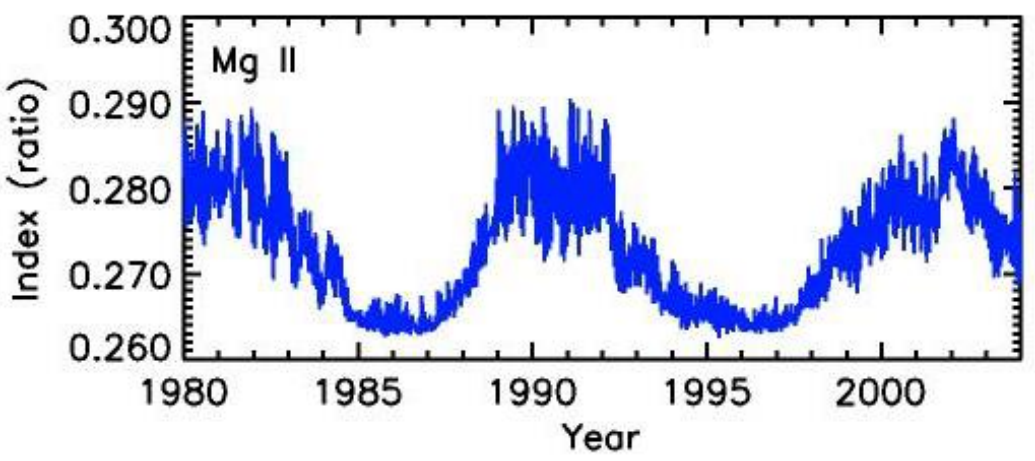


Frohlich & Lean (2004)

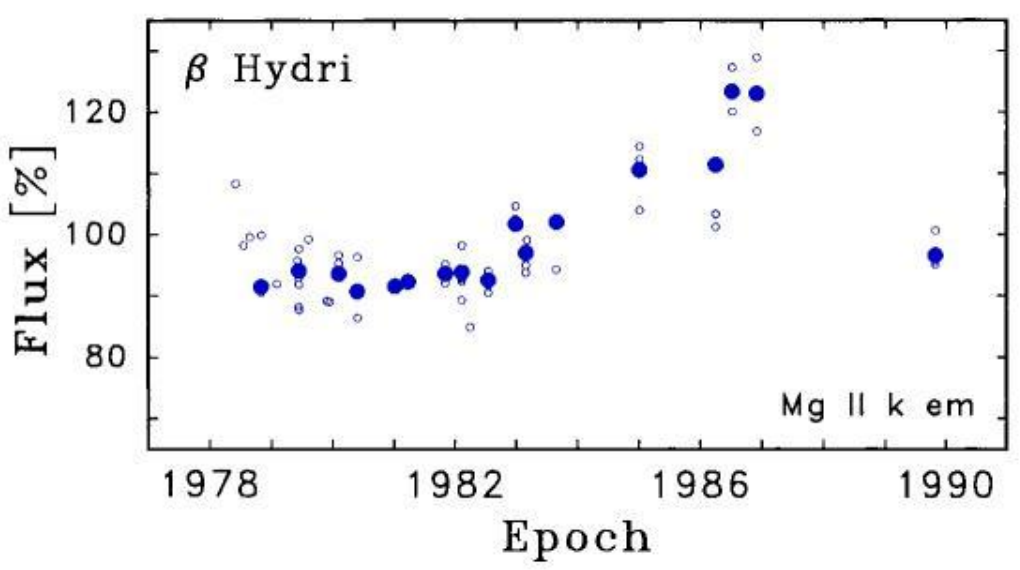


Dravins et al. (1993)

# FRAUNHOFER CaII H AND K LINES

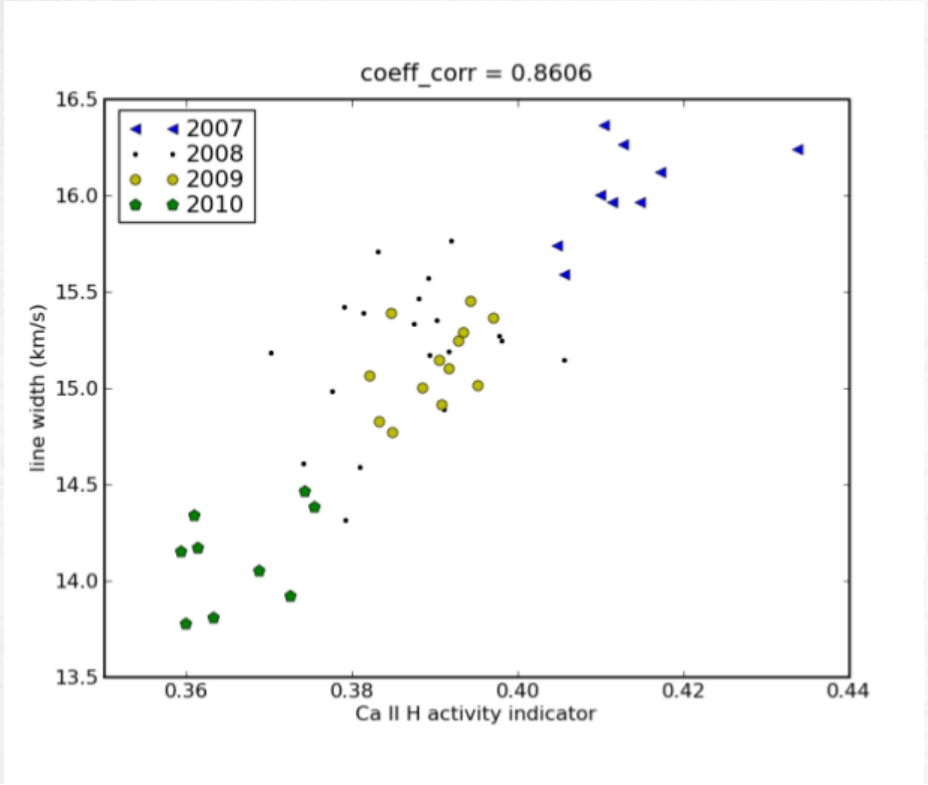


correlation between the widths of the FeI 846.84 nm magnetic line and the values of the CaII H index.

Morgenthaler et al. (2010)

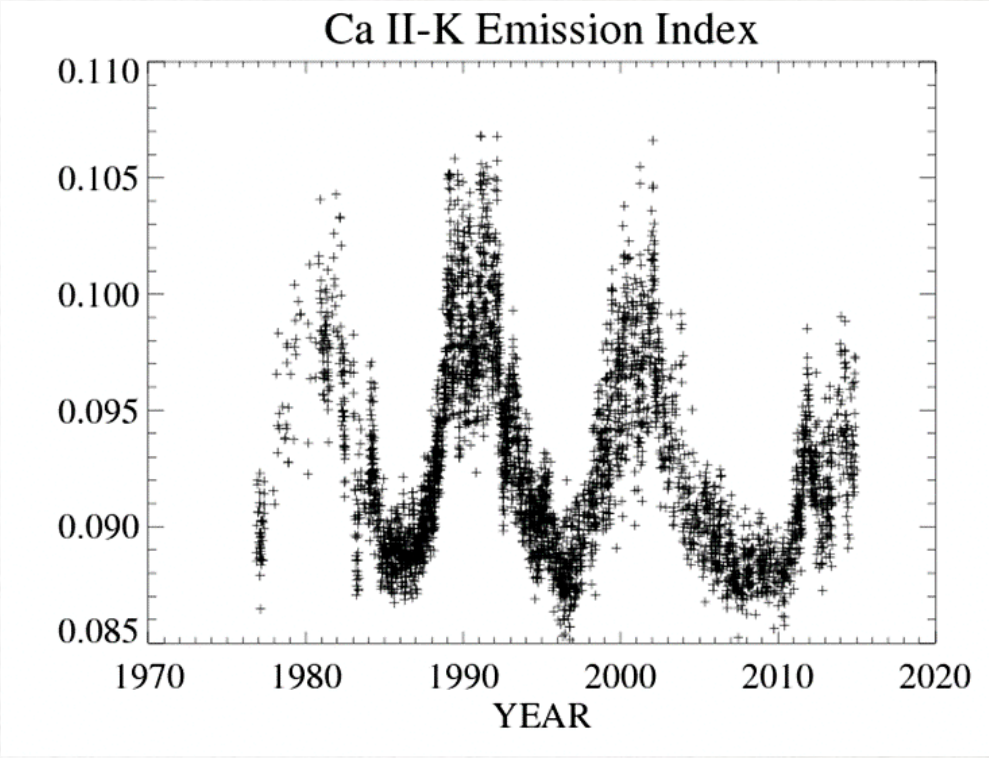


NSO - SACRAMENTO PEAK

# MT. WILSON SURVEY

- Systematic observations of stellar magnetic activity began in 1966, when Wilson (1968) began the ground-based "Mt. Wilson survey".
- Observation of Fraunhofer Ca II "H and K" lines at 397 and 393 nm, whose line cores form in chromospheric plasmas.

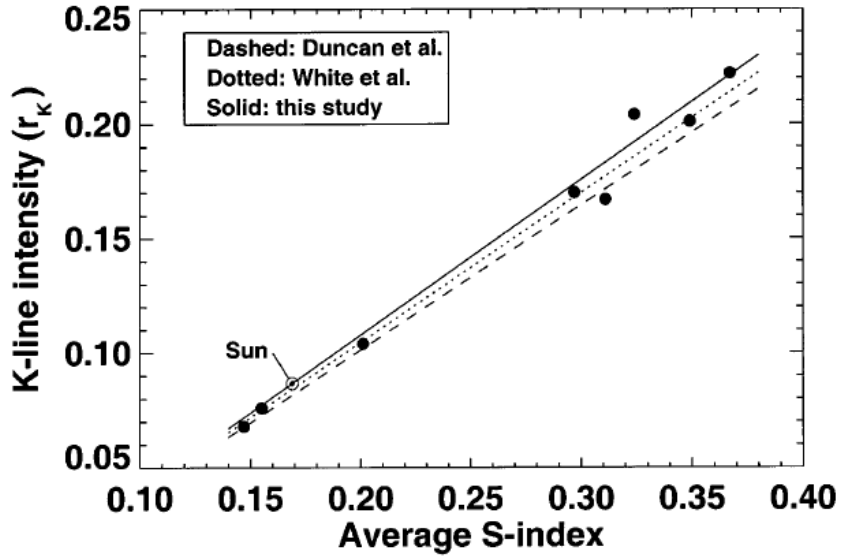


FIG. 2.—Solar and stellar data and three transformations for relating the solar *K*-index to the stellar *S*-index.

Radick et al. (1998)

# SUN IS A TYPICAL LOW-S STAR

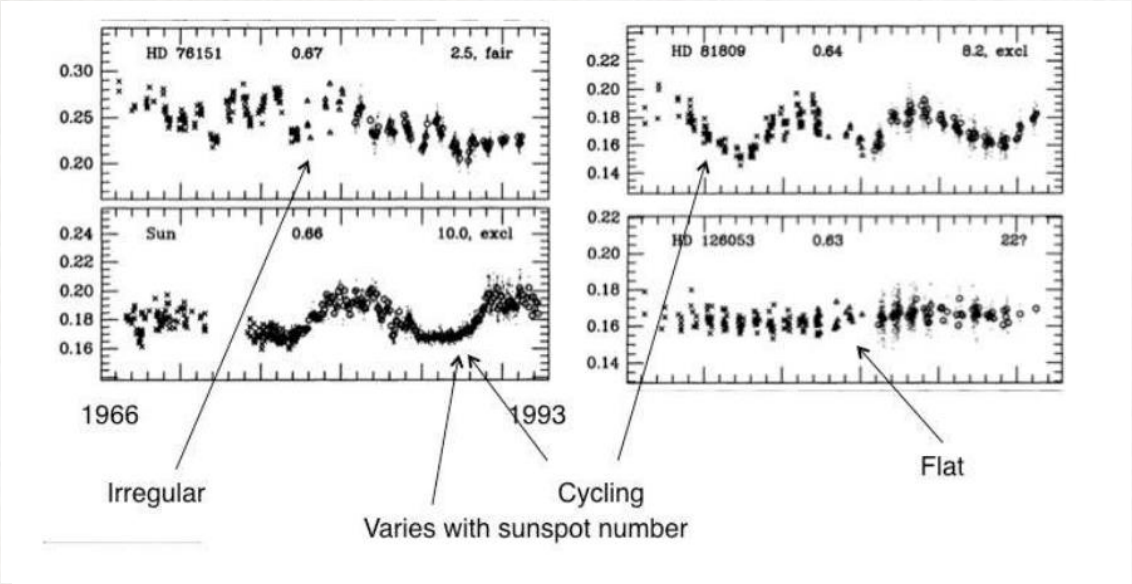


**Figure 3.** A selection of different stellar behavior measured in the Mt. Wilson survey up to 1995, reported by Baliunas et al. (1995). The upper four panels show representative time series of the "S-index", the lower panels the number of stars as a function of cycle period, and the number of stars which were classified as cyclic (C, like the current Sun), irregularly variable (V), flat (F, the Maunder Minimum Sun?) and with a long-term trend (L).

Judge & Thompson (2012)

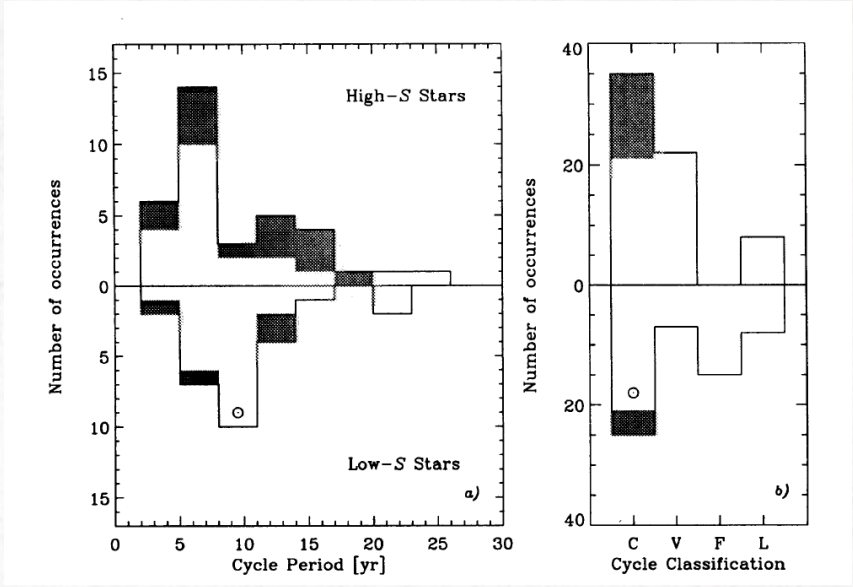


FIG. 3.—(*a*) The distribution of cycle periods (in 3 yr bins) for high-$\langle S \rangle$ (*upper histogram*) and low-$\langle S \rangle$ (*lower histogram*) stars (see text). Shaded areas represent secondary periods for stars where two periods were measured. The ⊙ symbol indicates the bin containing the Sun. (*b*) Similar to (*a*) except that the distribution of long-term activity classifications are shown: "C" cyclic (the shaded area shows additional secondary cycle periods), "V" variable, "F" flat (nonvarying), and "L" long-term trend.

Baliunas et al. (1995)

# SOFT X-RAY FLUX FROM SOLAR TYPE STARS

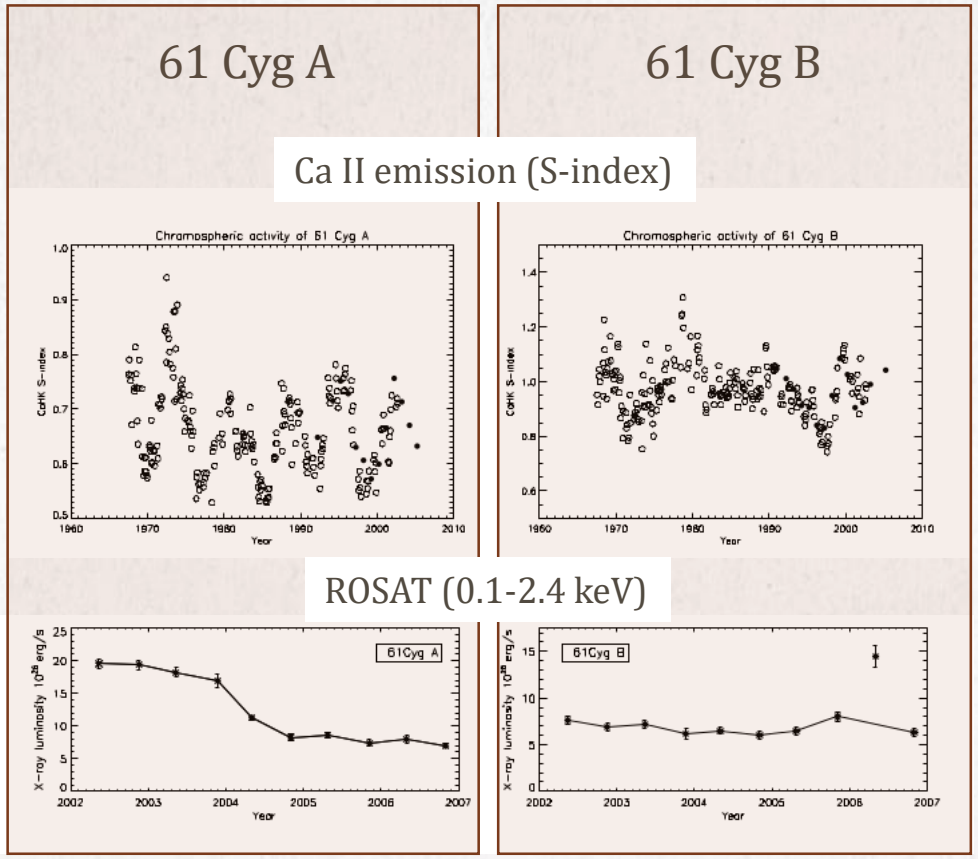

# „DISAPPEARANCE" OF THE CORONA OF THE α Cen A

XMM-Newton (0.2-2.0 keV)

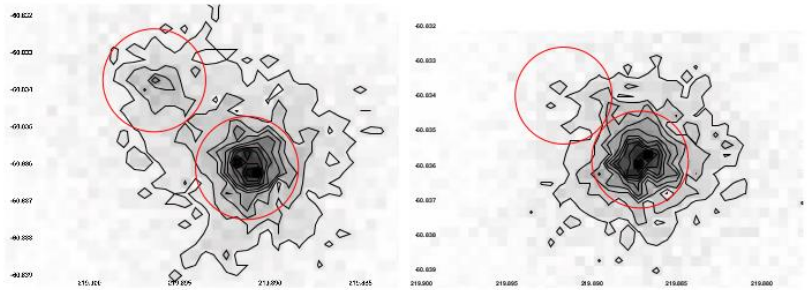

**Fig. 2.** The Alpha Centauri system observed with MOS1 during March 2003 (left) and February 2005 (right), overlayed are brightness contours and 5″ source regions (red) to indicate the proper motion. The X-ray darkening of $\alpha$ Cen A (upper left) is observed with XMM-Newton for the first time.

Robrade et al. (2007)

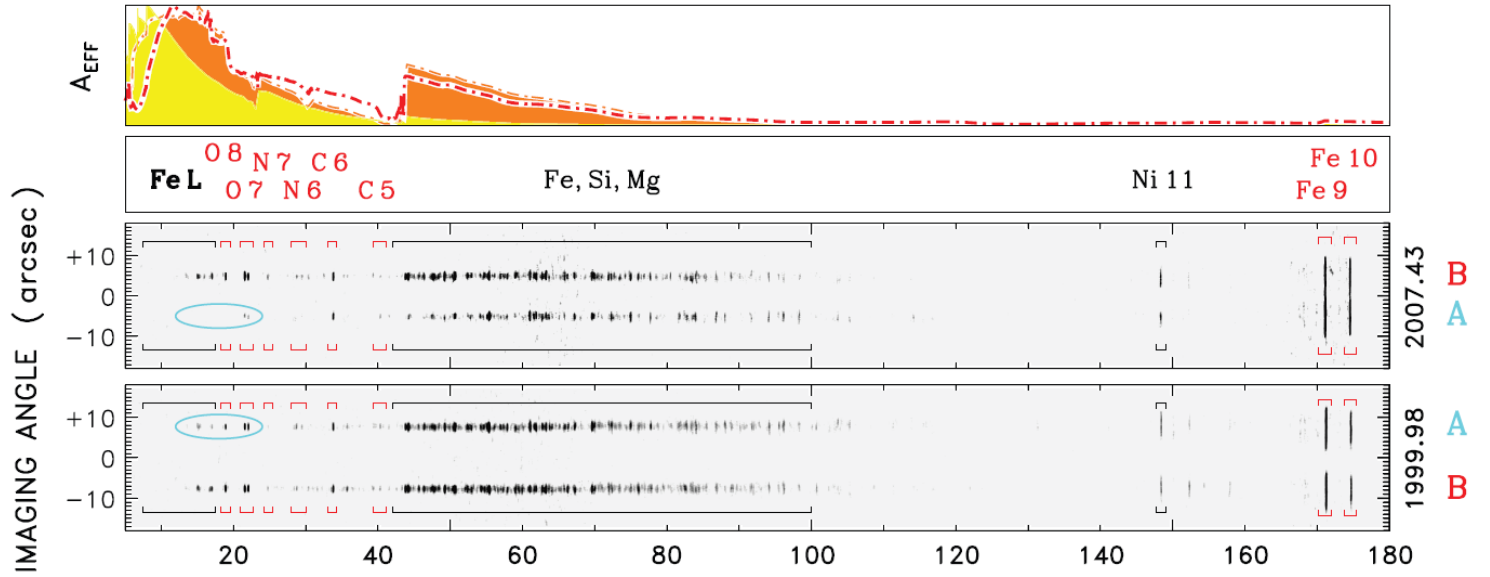


FIG. 2.—*Chandra* LETGS spectra of $\alpha$ Cen 7.5 years apart. The main panels illustrate the spatially resolved LETGS events, binned into an image combining the plus and minus grating arms. Owing to vignetting, the spectral stripes bloom toward longer wavelengths, and become slightly blended in the more recent LETGS exposure. Nevertheless, the short-wavelength portions of both spectra are cleanly resolved. The A component is the lower stripe in the upper spectrum, and the upper stripe in the lower one, owing to opposite roll angles in the two epochs. He-like and H-like CNO emissions are conspicuous in the 20–40 Å interval, while the Fe L-shell features below 20 Å are weak in these relatively cool (1–2 MK) coronal sources. Si, Mg, and Fe M-shell emissions crowd the 40–100 Å interval, and the isolated Fe IX and Fe X lines beyond 170 Å are very bright. The A and B spectra in the earlier observation (1999.98) are quite similar to one another, and to the 2007.43 trace of the B component. The new A spectrum, however, displays a striking lack of emission below 30 Å (highlighted by blue ovals in both epochs). The top panel compares normalized effective area curves of MOS 1 (with thick blocking filter; *yellow shading*), HRC-I (*orange shading*), and LETGS zeroth order (*red dot-dashed curve*). The *XMM-Newton* camera is sensitive mainly to emission below 0.3 keV (40 Å), whereas the *Chandra* detectors have extended soft response.

Chandra spectra – Ayres et al. (2008)

# STELLAR MAUNDER MINIMUM

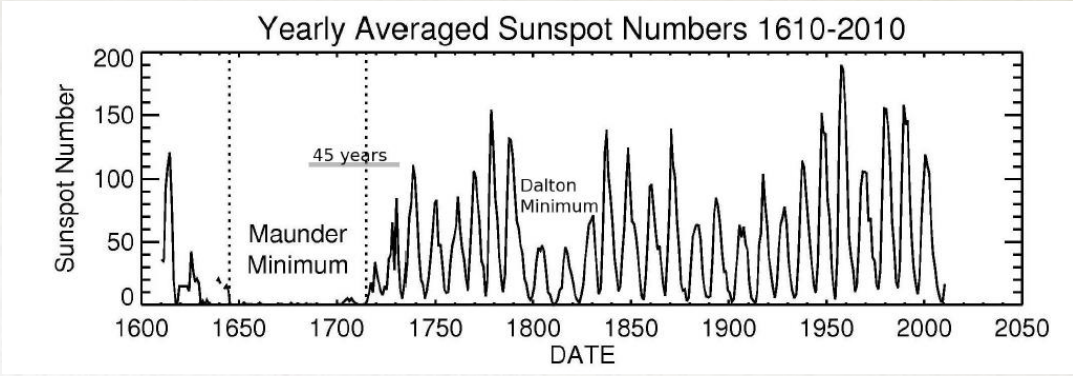


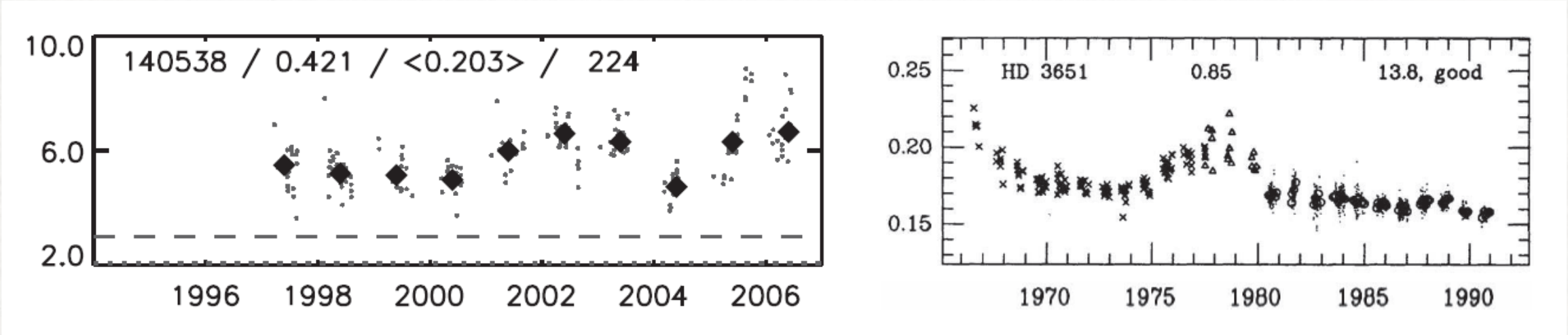


**Figure 17:** Left: HD 140538 appears to have made a transition from a flat activity state to an unusually short cycle in 2000 (from Hall *et al.*, 2007b). Right: HD 3651 shows evidence of having entered a flat activity state around 1980 (from Baliunas *et al.*, 1995).

Hall (2008)

# IS THE SUB-CONVECTION ZONE SHEAR LAYER ESSENTIAL COMPONENT OF THE DYNAMO?

Proxima Centauri

Cincunegui et al. (2007)

**Table 2.** Nightly averaged $A$ index. Column 1: the label used in Fig. 7; Col. 2: the xJD at the beginning of the observations; Col. 3: the quantity of spectra averaged; Col. 4: the total exposure time (in minutes); Col. 5: the average index.

| Label | xJD | $N$ | $t$ | $A$ |
|---|---|---|---|---|
| 0399 | 241.85 | 2 | 50 | 2.89 |
| 0300 | 627.82 | 2 | 90 | 2.50 |
| 0301_1 | 972.78 | 2 | 120 | 2.14 |
| 0301_2 | 974.70 | 2 | 180 | 2.00 |
| 0701 | 1 096.46 | 2 | 180 | 2.84 |
| 0302 | 1 364.69 | 1 | 45 | 2.16 |
| 0602 | 1 451.66 | 2 | 90 | 2.13 |
| 0802 | 1 519.50 | 1 | 45 | 2.84 |
| 0303_1 | 1 715.75 | 1 | 45 | 2.28 |
| 0303_2 | 1 716.60 | 7 | 420 | 2.63 |
| 0903 | 1 895.51 | 2 | 66 | 2.46 |
| 0604_1 | 2 160.59 | 2 | 90 | 2.35 |
| 0604_2 | 2 161.51 | 5 | 300 | 2.00 |
| 0904 | 2 274.48 | 2 | 60 | 2.48 |
| 0305 | 2 448.78 | 1 | 45 | 2.61 |
| 0605_1 | 2 523.55 | 6 | 360 | 2.46 |
| 0605_2 | 2 543.60 | 2 | 180 | 2.54 |
| 0805 | 2 600.51 | 2 | 160 | 2.66 |
| 0206 | 2 780.86 | 1 | 80 | 2.42 |

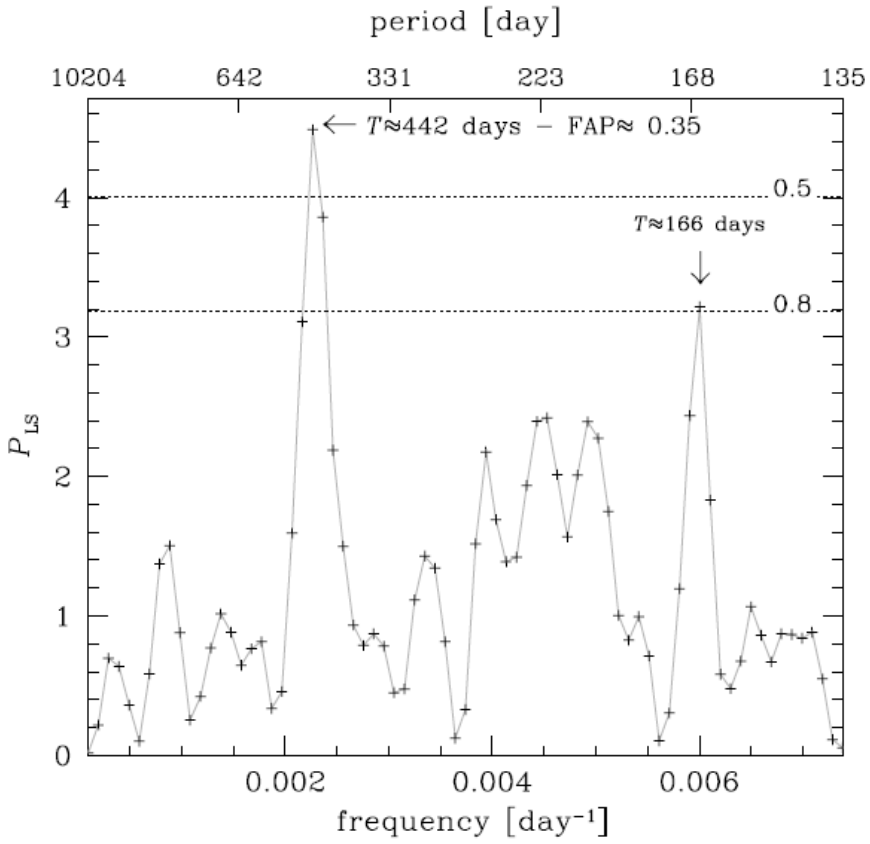


**Fig. 5.** Lomb-Scargle periodogram of the data of Table 2. The False Alarm Probability levels of 50 and 80% are shown.

# CYCLE PERIODS AGAINST ROTATION PERIOD

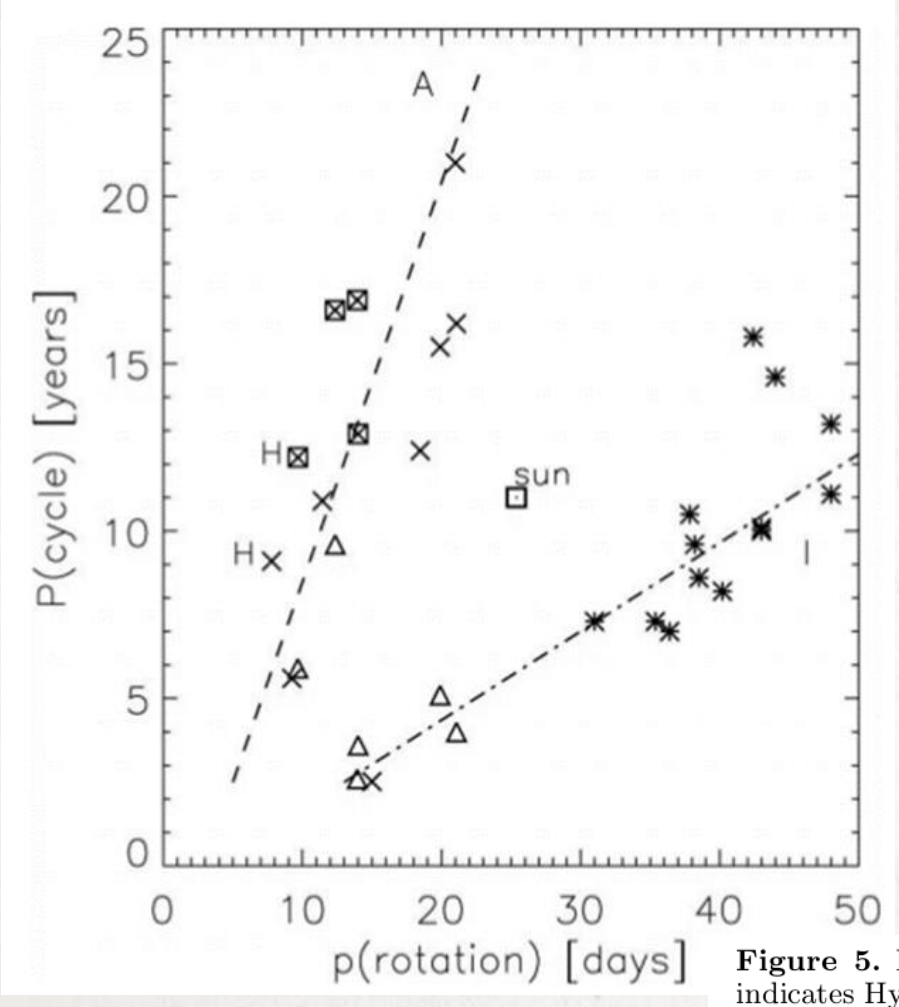


Data from Saar & Brandenburg (1999)

**Figure 5.** Periodic behavior derived from the Ca II S index data (Böhm-Vitense 2007). H indicates Hyades group stars, A and I active and inactive sequences. Squares show stars with B -V $< 0.62$. Triangles indicate secondary periods for stars on the A sequence.

# SOLAR-STELLAR CONNECTION

Understand dynamo and the interaction of rotation, convection and magnetic field

- Different physical conditions (rotation rate, depth of convection zone)
- Assuming dynamo operates similarly in solar-type stars compared to the Sun
- Constraints on solar dynamos:
  - Dynamos periods and activity levels scalings
  - Understand relative importance of tachocline and structure of the stars
- Predict solar cycles

# SOLAR CYCLE FROM THE ASTEROSEISMOLOGICAL POINT OF VIEW

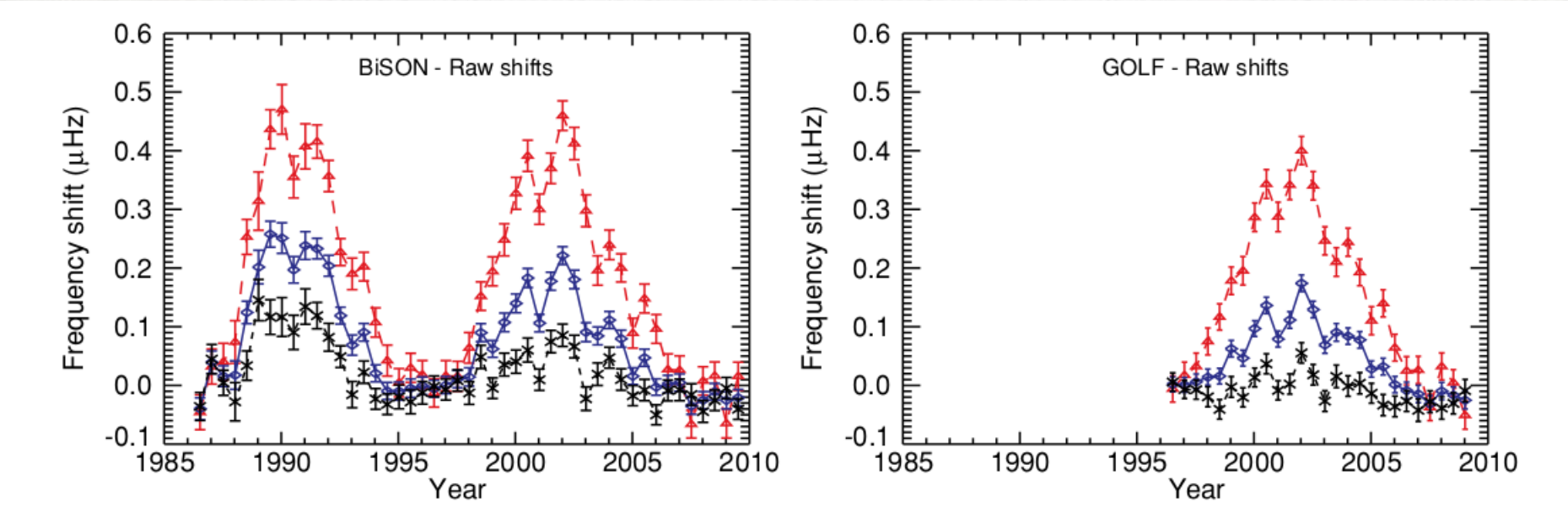


**Figure 1.** Top: average frequency shifts of "Sun-as-a-star" modes with frequencies between 1.88 and 3.71 mHz (total-frequency band, blue solid line, and diamond symbols); 1.88 and 2.77 mHz (low-frequency band, black dotted line, and cross symbols); and 2.82 and 3.71 mHz (high-frequency band, red dashed line, and triangle symbols).

Fletcher et al. (2010)

- Detection of activity even when no surface evidence (Salabert et al. 2009)

# SOURCES OF OSCILLATION FREQUENCY INCREASE WITH RISING SOLAR ACTIVITY

- For p-modes, the most plausible explanation of the frequency increase is a less than 2% decrease in the radial component of the turbulent velocity in the outer layers. Lower velocity implies a lower efficiency of the convective transport, hence lower temperature, which also contributes to the p-mode frequency increase.

Dziembowski & Goode (2005)

# CYCLE IN COROT TARGET HD 49933

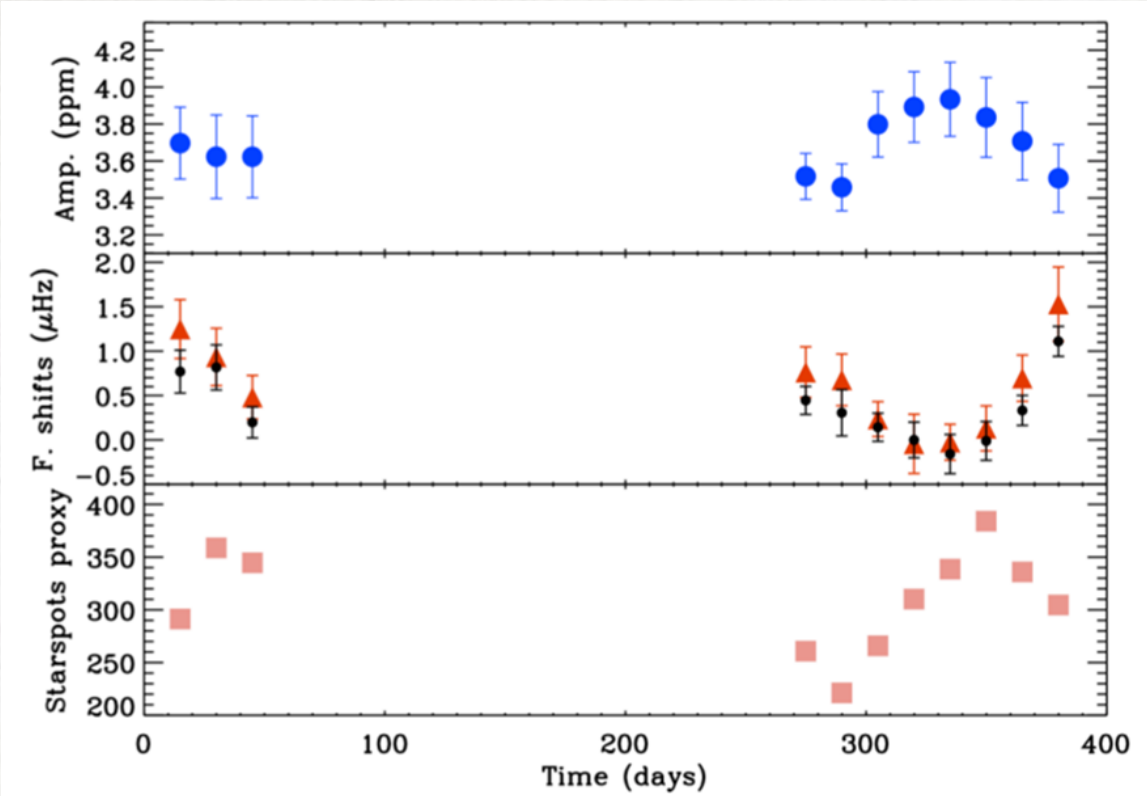


**Fig. 1.** Time evolution –beginning February 6, 2007– of the mode amplitude **(top)**, the frequency shifts using two different methods **(central)**: cross correlations (red triangles) and individual frequency shifts (black circles); and a starspot proxy **(bottom)** built by computing the standard deviation of the light curve (7). All of them are computed using 30-day long subseries shifted every 15 days (50% overlapping). The corresponding 1σ error bars are shown.

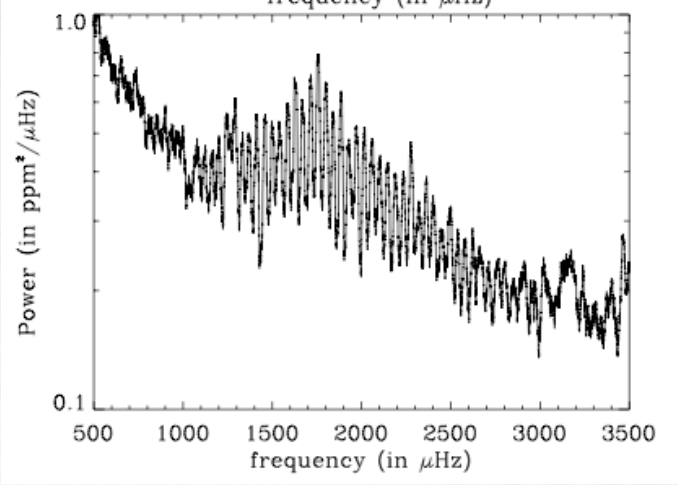


- Spectral type: F5V
- $P_{rot}$ = 3.4 days
- S-index ≈ 0.3 (active star)
- Observed by CoRoT during 60+137 days
- 50 oscillation modes measured

García et al. (2010)

# STELLAR ACTIVITY AND THE DETECTABILITY OF SOLAR-LIKE OSCILLATIONS

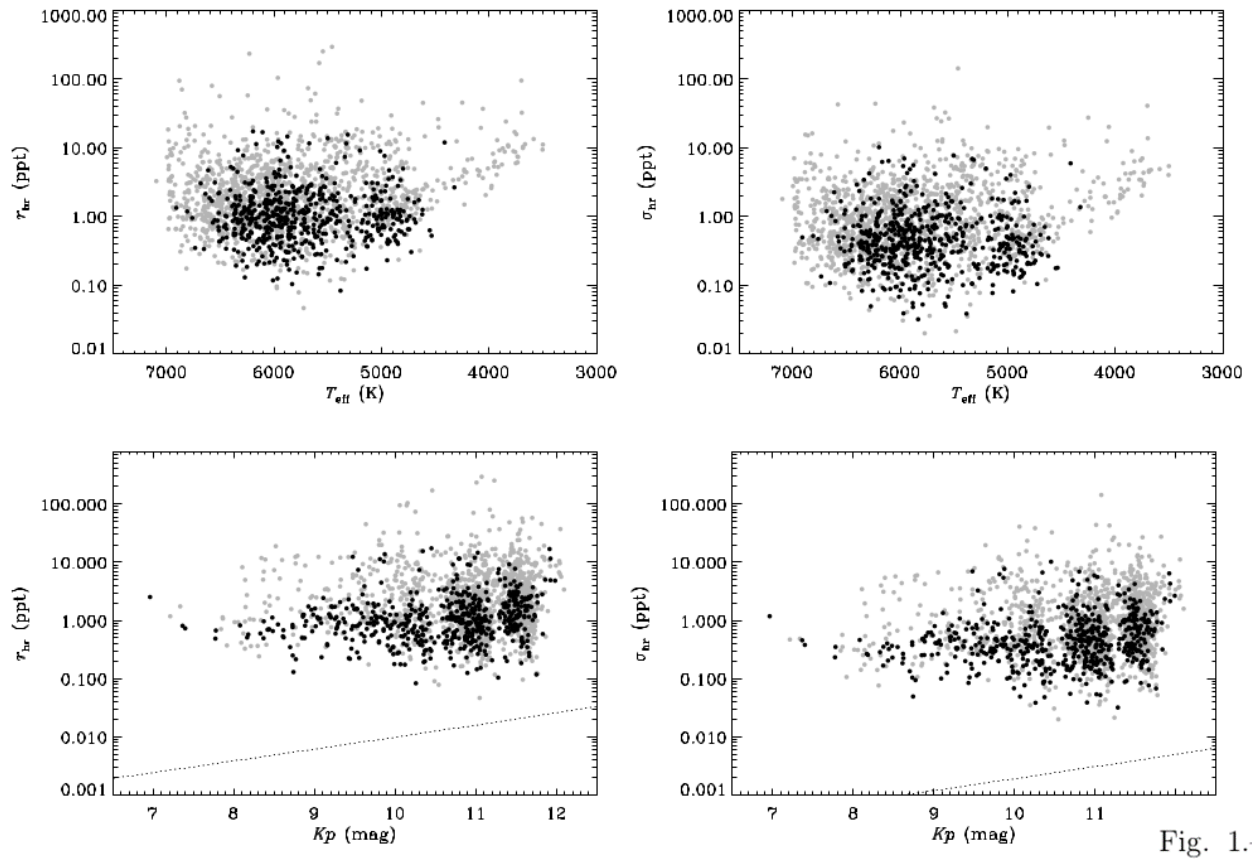


Chaplin et al. (2011)

Fig. 1.— Range, $r_{\rm hr}$, and RMS, $\sigma_{\rm hr}$ as a function of $T_{\rm eff}$ (top panels) and *Kepler* apparent magnitude, $Kp$ (bottom panels). Stars with detected solar-like oscillations are plotted in black; stars with no detections are plotted in gray. The dotted lines follow the additive corrections that were applied to $r_{\rm hr}$ and $\sigma_{\rm hr}$ (see text).

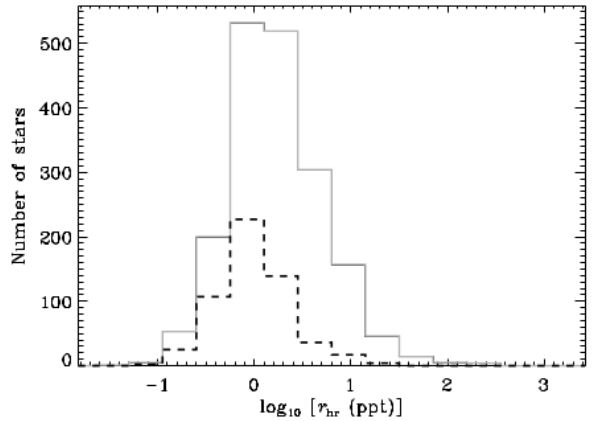


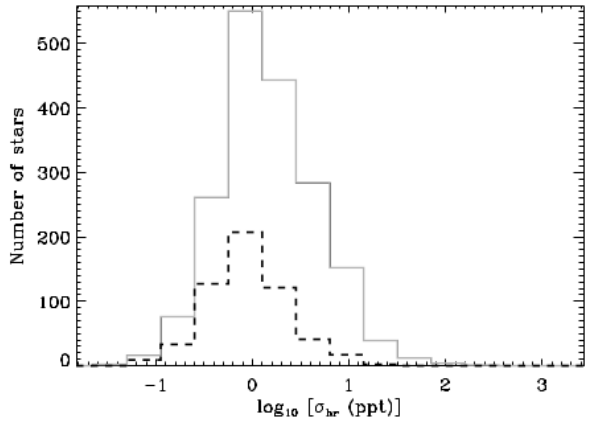


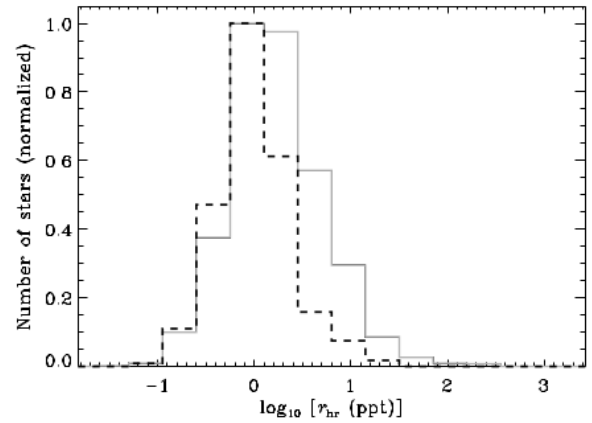


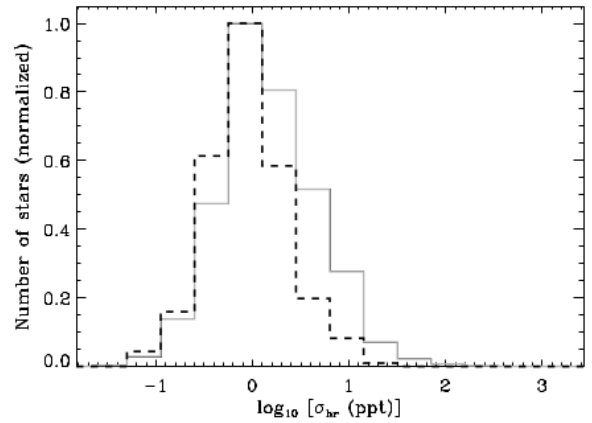


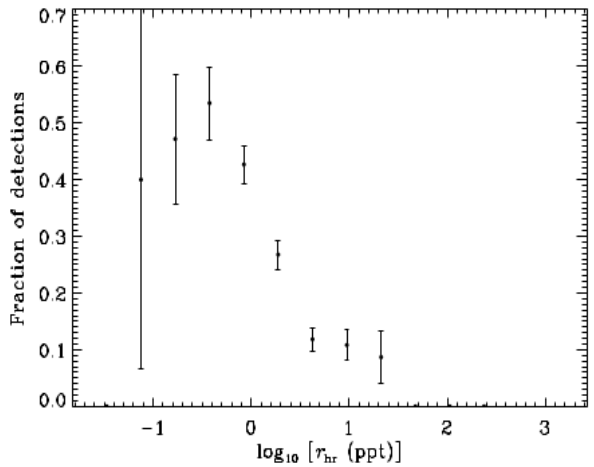


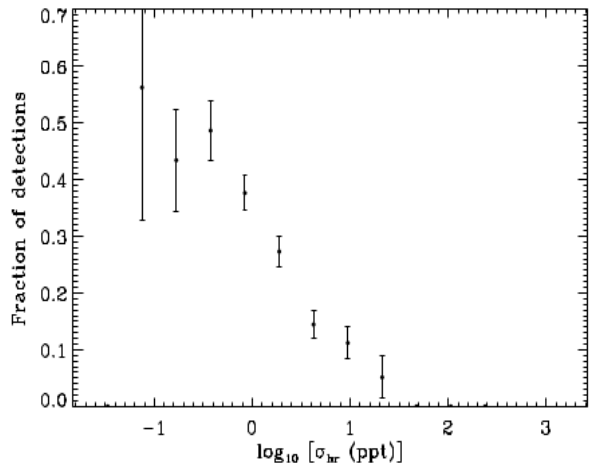


Top panels: Histograms of $r_{hr}$ and $\sigma_{hr}$, for all analyzed stars (gray solid lines) and stars with detected solar-like oscillations (black dashed lines).

Middle panels: Histograms normalized to a maximum value of unity (same line styles).

Bottom panels: Fraction of stars in each histogram bin showing detected solar-like oscillations.

Chaplin et al. (2011)

# STELLAR SPOTS AND TRANSITS OF PLANETS

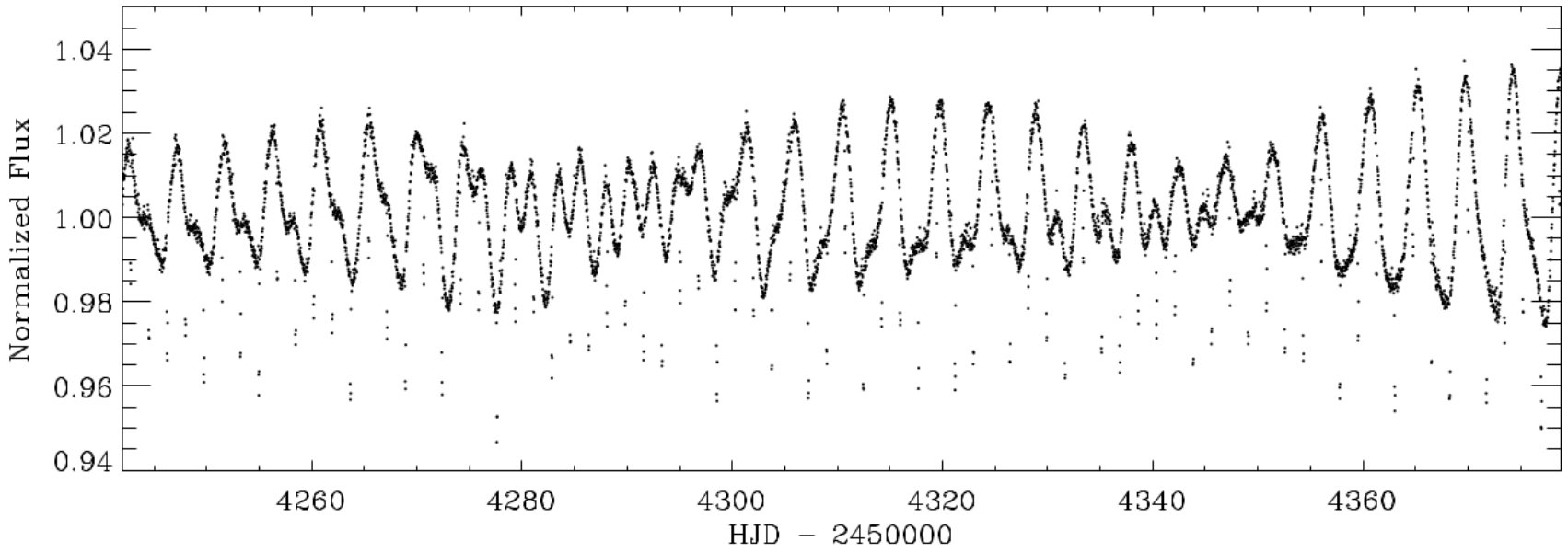


**Fig. 1.** Normalized flux of the CoRoT-Exo-2 star, showing a low frequency modulation due to the presence of spots on the stellar surface, and the 78 transits used to build the phase-folded transit of the Figure 2. For clarity purposes, data have been combined in 64-points bins (~34 min).

# STELLAR SPOTS AND TRANSITS OF PLANETS

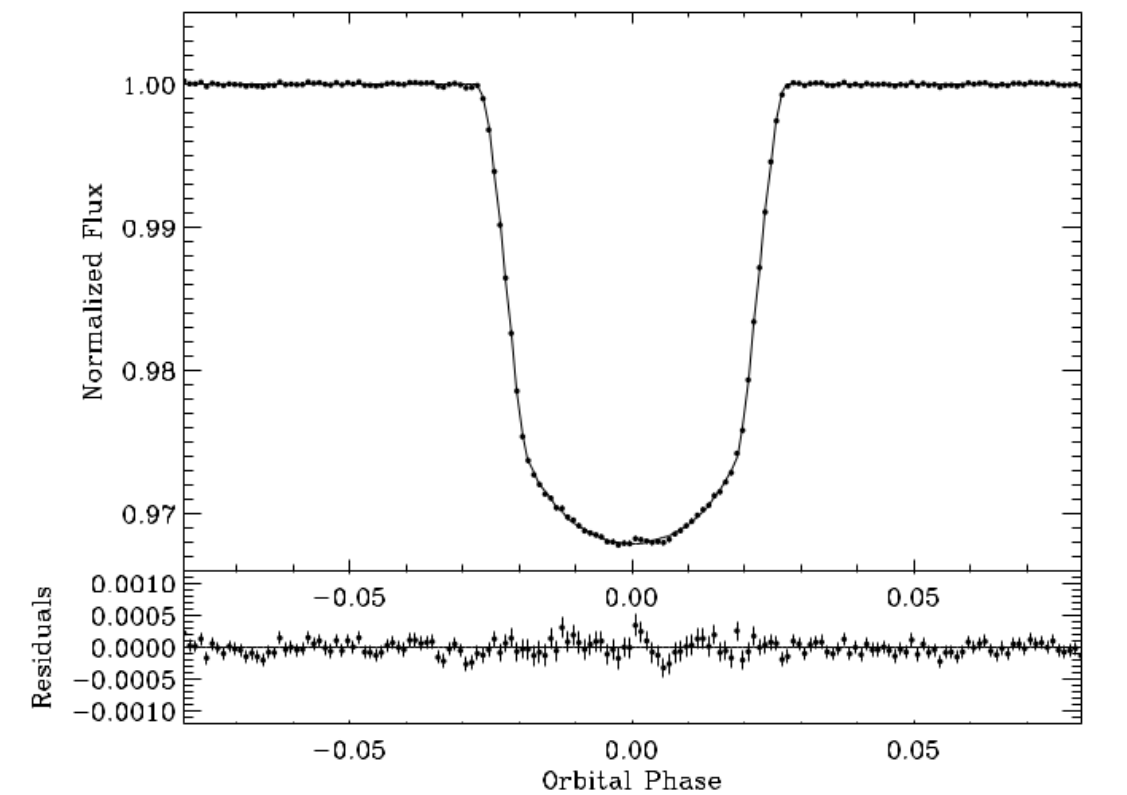


**Fig. 2.** Normalized and phase folded light curve of 78 transits of CoRoT-Exo-2b (top), and the residuals from the best-fit model (bottom). The bin size corresponds to 2.5 min, and the 1-sigma error bars have been estimated from the dispersion of the points inside each bin. The residuals of the in-transit points are larger due to the effect of successive planet occultations of stellar active regions.

# CONCLUSIONS

- The Sun lies at an overall low level of magnetic activity for a star of its spectral type, but its activity appears normal for a star of its age.
- We must continue to get much more “boring” data, monitoring the photometric and Ca II emission for decades into the future.
- Asteroseismology with Kepler and other experiments will clarify the evolutionary states of large numbers of stars.
- We must observe in detail “solar twins,” e.g. 18 Sco and 16 Cyg (Metcalfe et al. 2012).